



HAL
open science

The source of the threading dislocation in GaSb/GaAs hetero-structures and their propagation mechanism

Y. Wang, P. Ruterana, S. Kret, S. El Kazzi, L. Desplanque, X. Wallart

► To cite this version:

Y. Wang, P. Ruterana, S. Kret, S. El Kazzi, L. Desplanque, et al.. The source of the threading dislocation in GaSb/GaAs hetero-structures and their propagation mechanism. Applied Physics Letters, 2013, 102, pp.052102-1-5. 10.1063/1.4790296 . hal-00795953

HAL Id: hal-00795953

<https://hal.science/hal-00795953>

Submitted on 27 May 2022

HAL is a multi-disciplinary open access archive for the deposit and dissemination of scientific research documents, whether they are published or not. The documents may come from teaching and research institutions in France or abroad, or from public or private research centers.

L'archive ouverte pluridisciplinaire **HAL**, est destinée au dépôt et à la diffusion de documents scientifiques de niveau recherche, publiés ou non, émanant des établissements d'enseignement et de recherche français ou étrangers, des laboratoires publics ou privés.

The source of the threading dislocation in GaSb/GaAs hetero-structures and their propagation mechanism

Cite as: Appl. Phys. Lett. **102**, 052102 (2013); <https://doi.org/10.1063/1.4790296>

Submitted: 16 November 2012 • Accepted: 21 January 2013 • Published Online: 04 February 2013

Yi Wang, P. Ruterana, S. Kret, et al.



View Online



Export Citation



CrossMark

ARTICLES YOU MAY BE INTERESTED IN

[Strain relief by periodic misfit arrays for low defect density GaSb on GaAs](#)

Applied Physics Letters **88**, 131911 (2006); <https://doi.org/10.1063/1.2172742>

[Mechanism of formation of the misfit dislocations at the cubic materials interfaces](#)

Applied Physics Letters **100**, 262110 (2012); <https://doi.org/10.1063/1.4731787>

[Interfacial misfit array formation for GaSb growth on GaAs](#)

Journal of Applied Physics **105**, 103104 (2009); <https://doi.org/10.1063/1.3129562>

Lock-in Amplifiers
up to 600 MHz



Zurich
Instruments



The source of the threading dislocation in GaSb/GaAs hetero-structures and their propagation mechanism

Yi Wang,^{1,a)} P. Ruterana,^{1,b)} S. Kret,² S. El Kazzi,³ L. Desplanque,³ and X. Wallart³

¹CIMAP, CNRS UMR 6252, 6, Boulevard du Maréchal Juin, 14050 Caen Cedex, France

²Institute of Physics, PAS, AL. Lotników 32/46, 02-668 Warszawa, Poland

³IEMN, UMR-CNRS 8520, BP 60069, 59652 Villeneuve d'Ascq Cedex, France

(Received 16 November 2012; accepted 21 January 2013; published online 4 February 2013)

The misfit and threading dislocations during GaSb epitaxy on GaAs substrate were investigated by weak beam dark field and high angle dark field scanning transmission electron microscopy. The geometric phase analysis and dislocation density tensor analysis were next used to analyze the strain around the threading dislocations and quantify the corresponding Burgers vectors. It is shown that there are three types of threading dislocations (mixed, edge, and pair of mixed types) close to the interface, which originate from the 60°, Lomer, and 60° pair misfit dislocations, respectively. During the growth of the epitaxial layer, the edge type as well as the pair of mixed threading dislocations split into two mixed type dislocations for the glide in {111} planes. Eventually, only mixed type dislocations have been observed at the surface of thick GaSb layers.

© 2013 American Institute of Physics. [<http://dx.doi.org/10.1063/1.4790296>]

The epitaxy of the Sb-based III-V semiconductor on GaAs (or Si, GaP) is of great interest for applications in the near- and far-infrared optoelectronics and ultra-high speed low-power consumption electronics.¹ Given the large lattice mismatch between the epitaxial layer and substrate (for instance 7.8% for GaSb/GaAs), the critical thickness is expected to be only a couple of monolayers (MLs); afterwards, misfit dislocations are expected to form rapidly. In these systems, with substantial mismatch, the misfit dislocation arrays comprises Lomer as well as 60° dislocations²⁻⁵ and are not perfect.^{2,3} Therefore, increasing the epitaxial layer thickness leads to the formation of threading dislocations that propagate in the epitaxial layer to the top active layers where they are known to limit the performance of the devices.⁶ It has been reported that in large lattice mismatch the Lomer dislocation with Burgers vector of $\frac{a}{2}\langle 110 \rangle$ is the predominant misfit dislocation.^{2,4} In the GaSb/GaAs system, if all of the lattice mismatch strain was to be relieved by Lomer dislocations, a cross grid network of parallel misfit dislocations lying in the [110] and $[1\bar{1}0]$ directions with a spacing of 5.51 nm would be expected, and in such a case, the threading dislocations could be entirely avoided.⁷ This is the concept of the so-called "IMF" (interfacial misfit) growth which has been more recently proposed and shown in some instances to be particularly successful in reducing the dislocation densities by more than three orders of magnitude from the more usual 10^8 - 10^9 cm⁻² to about 10^5 cm⁻².⁸ However, the Lomer dislocation network cannot be perfect and the threading dislocations are almost always present.⁹ Regarding the source of the threading dislocations, it is generally accepted that the 60° misfit dislocations are the primary source of the threading dislocation. They are either nucleated at the growth surface of the film and glide into the interface along the {111} slip planes¹⁰ or introduced during the island

coalescence at the later stages of growth.¹¹ However, Kang *et al.* have reported that the Lomer dislocation propagates directly to the film surface at low growth temperature (420 °C) in GaSb/GaAs.¹² Besides the 60° and Lomer dislocation, 60° dislocation pairs have also been observed,^{10,13} and their role in the formation of threading dislocations is not clear. Moreover, it appears that the propagation of threading dislocations in the epitaxial layer has not yet been deeply investigated and their structural evolution on the way towards the surface is still unclear.

In this work, the source and the propagation of the threading dislocations in the GaSb epitaxial layer grown on GaAs substrate were investigated by the weak beam dark field (WBDF) and high-angle dark-field (HAADF) scanning transmission electron microscopy (STEM). The propagation mechanism of the threading dislocations was analyzed through a series of samples with different epitaxial layer thickness.

The samples were grown by molecular beam epitaxy (MBE) with a base pressure better than 1×10^{-10} Torr. After the deoxidization of the GaAs substrate at 625 °C under an As flux, a 300 nm GaAs layer was first grown at 580 °C to smooth the surface. Then, the Ga and As valves were closed, and the sample temperature was decreased to 460 °C. After an exposure to Sb flux, the (1×3) surfaces reconstructions of GaAs was generated as monitored by *in situ* reflection high-energy electron diffraction. Following the (2×8) substrate surface reconstructions, GaSb with different thickness (27 MLs, 100 MLs, 300 MLs, and 600 nm) was deposited. The growth rate was 0.7 ML/s for the GaSb layers with a Sb flux of 2.5 ML/s. The plane-view samples were prepared by a standard procedure including grinding, and dimpling and final argon ion beam milling in a stage cooled with liquid nitrogen. The WBDF analysis was carried out on JEOL 2010 LaB₆ microscope operated at 200 kV. The Z contrast HAADF images were acquired using a FEI Titan 80-300 Cubed Microscope equipped with an objective spherical aberration (C_s) corrector operated at 300 kV, along [001] zone axis.

^{a)}Electronic mail: yi.wang@ensicaen.fr.

^{b)}Electronic mail: pierre.ruterana@ensicaen.fr.

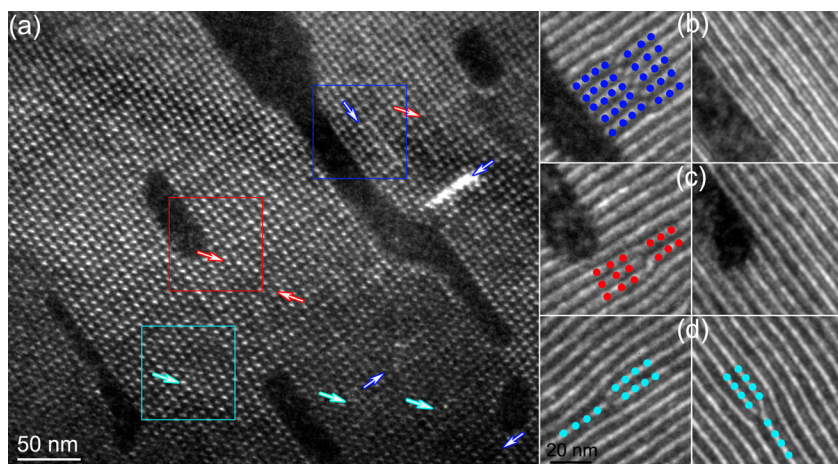


FIG. 1. (a) The WADF images of 27 MLs GaSb grown on (001) GaAs at 460 °C showing the 2D network of the misfit dislocations observed at $g/3g$ condition with $g=040$, the imperfections have been marked by the arrows. (b), (c), and (d) showing the details of three types of imperfections, each of them was observed with $g=220$ and 220 respectively. Note the imperfection 1 (blue) comes from 60° dislocation, imperfection 2 (red) originates from Lomer dislocation, and imperfection 3 (cyan) is from 60° dislocations pair.

With the help of WADF technique we are able to image the misfit dislocation network. As shown in Fig. 1(a), the two families of Lomer misfit dislocation array in the sample with 27 MLs GaSb were observed in weak beam $g/3g$ condition with $g=040$. In perfect areas the interface shows ideal misfit dislocation network and consists solely of Lomer dislocations. However, some defects (or imperfections) of the Lomer dislocation network marked by the arrows can also be noticed. These imperfections have been reported to be the source of the threading dislocations.¹² At first glance, two types of imperfections are in the interface: (1) half period shift of Lomer dislocation resulting from the interaction of 60° dislocation (blue arrow); (2) an extra Lomer dislocation (red arrow). The details of these imperfections can be interpreted using the $g/3g$ WADF condition with $g=220$ by which we can image the two families of misfit dislocations separately. Figs. 1(b) and 1(c) show the WADF image of the highlighted area of Fig. 1(a) observed close to $2\bar{2}0$ and 220 diffraction condition. The details of these imperfections are highlighted by dotted lines. In Fig. 1(b), the $2\bar{2}0$ type misfit dislocations have a half period shift along $[110]$ direction and the 220 type misfit dislocation are perfect; in Fig. 1(c), the extra Lomer dislocations appear in $2\bar{2}0$ type misfit dislocation and the 220 type misfit dislocation are perfect too (note the two Lomer type threading dislocations in this area). Besides the above two imperfections that have been already reported before, an additional imperfection has been systematically observed (Fig. 1(a), cyan arrows). One of them (cyan square) has been analyzed in Fig. 1(d). In contrast to Figs. 1(b) and 1(c), extra half fringes are seen in both $2\bar{2}0$ and 220 diffraction conditions. Then, when closely looking at the core of the dislocation in Fig. 1(d) (left), in comparison to the Lomer case in Fig. 1(c), it can be noticed that the fringes do not bend around the core, they split like in Fig. 1(b) (left),

although at a smaller extension (only the two fringes around the core).

The half period shift of Lomer dislocation has been attributed to: (1) the interaction of a 60° dislocation which results from the coalescence of islands with the Lomer dislocation network;^{9,14} (2) the intersection of antiphase boundaries caused by the atomic surface steps.^{15,16} In our case, the growth starts on (001) GaAs substrate and no antiphase domain boundary was observed. Thus, the half period shift of Lomer dislocation network should originate from the 60° dislocation. Subsequently, the 60° dislocation bends its line into the growth direction, becoming a threading dislocation. Similarly, the extra Lomer dislocations cannot terminate at the interface and they should propagate to the surface of the film.¹² This is in contrast to the general opinion which considers that the Lomer dislocations are not likely to introduce any threading segments since they cannot glide on the close packed $\{111\}$ planes.^{9,17}

Given the different misfit dislocation network imperfections, different threading dislocations are to be expected: mixed types threading dislocation, which originated from the 60° dislocation and edge type threading dislocation, which come from the extra Lomer misfit dislocation, and a typical signature from the third imperfection. Along the $[001]$ zone axis at low magnification, we have also identified three types of additional fringes in the moiré fringes images of GaSb/GaAs interface (Fig. 2): 2 extra half moiré fringes at 90° , 2 parallel half moiré fringes, and 4 extra half moiré fringes. We then assumed that the three characters should be uniquely connected to the imperfections of the misfit dislocations and subsequent threading dislocations, and then zoomed in at each type of imperfection using HAADF-STEM. Figure 3(a) shows HAADF image of threading dislocation observed along the $[001]$ direction in the 100 ML sample. Since the

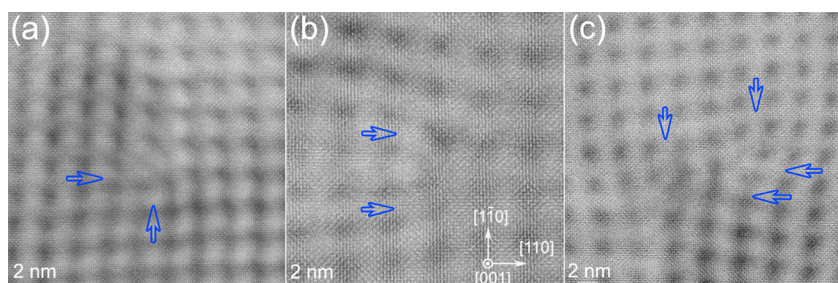


FIG. 2. The moiré fringes of GaSb/GaAs around the defect (or imperfection) of the misfit dislocation network observed in STEM along $[001]$ zone axis, the extra half moiré fringes in (a), (b), and (c) relate to 60° dislocation, Lomer dislocation, and 60° dislocations pair, respectively.

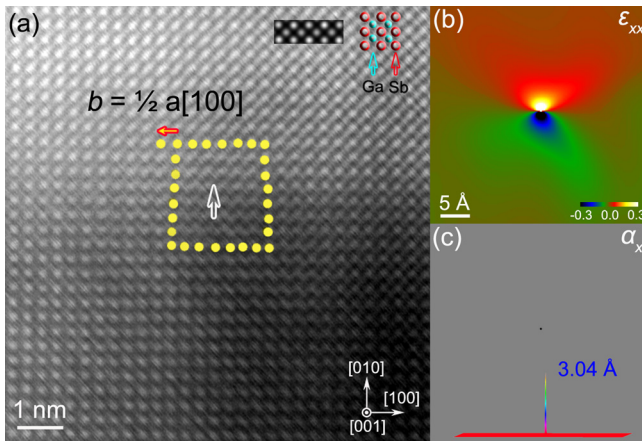


FIG. 3. (a) The HAADF image of mixed type threading dislocation with the projected Burgers Vector of $b = \frac{a}{2}[100]$ viewed along the $[001]$ direction, the additional $\{100\}$ plane was marked by the arrow, the inset of (a) shows the simulated HAADF image; (b) Strain field ϵ_{xx} obtained by GPA from (a); (c) dislocation density tensor α_x component (the α_y component is zero), the inset shows the corresponding 3D representation of α_x component.

image intensity in HAADF image is approximately proportional to the square of the atomic number (Z) in the 1s approximation,^{8,18,19} the spots with higher intensity correspond to the Sb atomic columns, as confirmed by the inset of Fig. 3(a) showing the simulated HAADF image of bulk GaSb with a thickness of 60 nm, using the QSTEM software.²⁰ As can be seen from the figure, the visible threading dislocation has only one $\{100\}$ additional plane. By drawing Burgers circuits, the Burgers vector was determined to be $\frac{a}{2}[100]$. Since we find that the investigated threading dislocation is not accompanied by a stacking fault, this indicates that we are observing a projection of a perfect dislocation. Using the geometrical phase analysis (GPA)^{21,22} we measured the strain field around the dislocation core region. Figure 3(b) shows the ϵ_{xx} strain component, with a reference to the bulk area. The strain gives a perfect shape of edge type dislocation strain field which is positive and tensile in the region above the dislocation core, negative and compressive below the dislocation core. Besides the strain distribution, we can also extract the dislocation density tensor from these strain fields.^{10,23} Figure 3(c) shows the α_x component of the dislocation density tensor of the investigated dislocation presented in Fig. 3(a). The bright/dark dot presents the maximal deformation area and mark the origin of the extra $\{100\}$ plane. The corresponding 3D representations of the α_x component at core region are inserted in Fig. 3(c). Integrating the α_x component in the dislocation core region yields 3.04 Å, whereas the α_y component is zero. So, the $[001]$ projection gives an edge component of $\frac{a}{2}[100]$ for this dislocation, which is not a translation vector for the structure. Therefore, this dislocation should have a component along the $[001]$ direction, which makes it a mixed type (or 60°) one.

Figure 4(a) shows HAADF image of another type of threading dislocation, which exhibits two $\{100\}$ additional planes giving a Burgers vector of $\frac{a}{2}[110]$. Figure 4(b) shows HAADF image of the third type of threading dislocation, which has two parallel $\{100\}$ additional planes giving a total Burgers vector of $a[100]$. The dislocation density tensor analysis shows that the dislocation in Fig. 4(a) has equal x

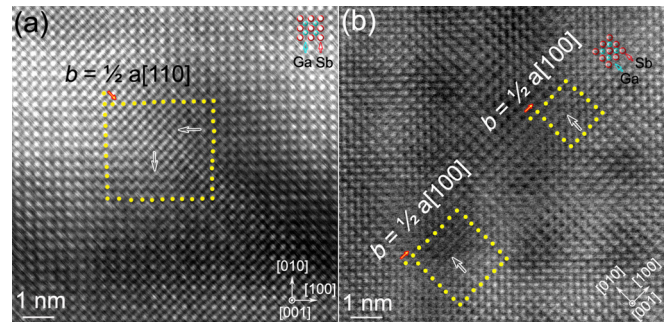


FIG. 4. (a) The HAADF image of edge type threading dislocation with the projected Burgers Vector of $b = \frac{a}{2}[110]$ viewed along $[001]$ direction; (b) the HAADF image of two mixed type threading dislocations with superimposed projected Burgers vector of $b = a[100]$ originated from 60° misfit dislocation pairs, in these images the additional $\{100\}$ planes have been marked.

and y component: 3.05 Å giving a Burgers vector of 4.3 Å. In Figure 4(b), the total Burgers vector is 6.09 Å is equal to $a[100]$. These measured values are in agreement with the Burgers circuits. Going back to imperfections at the misfit dislocations, we can conclude that the threading dislocations in Fig. 4(a) come from a Lomer dislocation since they have identical Burgers vector along $[110]$ or $[1\bar{1}0]$ direction, without a $[001]$ component. The dislocations in Fig. 4(b), which are observed as coming from the third type of imperfection, are two 60° dislocations (see Fig. 3). However, as seen from Figs. 1(d) and 2(c), they come from the same point at the interface. Therefore, these threading dislocations originate from one 60° dislocations pair.

The same observations and analysis have been carried out on the thicker epitaxial layer (300 MLs and 600 nm): in the sample with 300 MLs of GaSb, the dislocations coming from the three types of imperfections have also been observed. However, we systematically noticed that for the edge type threading dislocation as well as for the threading dislocations originating from 60° dislocations pair, the distance between the two core or initiation of the $\{100\}$ additional half lattice planes is always larger than that in the 100 MLs thick sample. Finally, in the sample of 600 nm thick sample, only isolated mixed type (60°) threading dislocations were observed.

It should be straightforward that the 60° dislocation will result in threading dislocation since both its Burgers vector and dislocation line lie in $\{111\}$ planes and it can easily glide along the $\{111\}$ plane. Given the geometry of the 60° misfit dislocation, for instance, a 60° dislocation with a Burgers vector of $\frac{a}{2}[101]$ and a dislocation line along the $[1\bar{1}0]$ direction, after propagation into the epitaxial layer, the dislocation line slips in the $\{111\}$ planes and the Burgers vector remains $\frac{a}{2}[101]$. Therefore, in plane-view observations, we are only able to observe the $\frac{a}{2}[100]$ edge component, as schematically shown in Fig. 5(a). The Lomer dislocation whose Burgers vector and dislocation line do not lie in a $\{111\}$ plane is sessile;²⁴ therefore, its propagation should follow a climb mechanism if it needs to keep the $[001]$ line direction. As compared with the glide in the slip plane, climb is not energetically favorable,²⁴ and looking at the above observations, the Lomer dislocations dissociate into two 60° dislocations. For instance, a Lomer dislocation with a Burgers vector of $\frac{a}{2}[110]$, may give rise to two 60° dislocations with Burgers

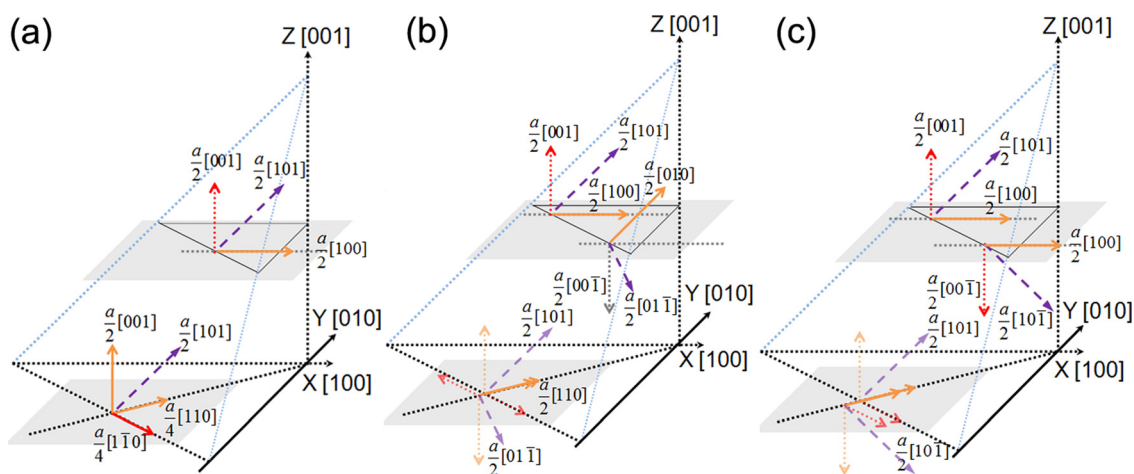


FIG. 5. The schematic geometry of the Burgers vector of the different types of threading dislocations and their relationship with misfit dislocations: (a) mixed type threading dislocation from 60° misfit dislocation, (b) edge typed threading dislocation from a Lomer dislocation, (c) mixed type threading dislocations originated from a 60° dislocations pair. The blue arrow represents the Burgers vector of the 60° dislocation; the orange and red arrows show the edge and screw components of the Burgers vector.

vector of $\frac{a}{2}[101]$ and $\frac{a}{2}[01\bar{1}]$, respectively, as shown in Fig. 5(b). This can explain why in the 100 MLs thick sample, the two $\{100\}$ additional planes do not originate from one point; in 300 MLs, the distance of the two $\{100\}$ additional planes is even larger; and finally in 600 nm thick sample, only mixed type threading dislocations are observed. As we have shown in our previous work,¹⁰ the 60° dislocations pair is formed by two 60° dislocations with parallel $[110]$ screw components, which prohibits the formation of a pure Lomer dislocation at interface (Fig. 5(c)). For instance, two 60° dislocations with Burgers vectors of $\frac{a}{2}[101]$ and $\frac{a}{2}[10\bar{1}]$, at the interface, their total edge component along the $[110]$ projection direction is equal to a Lomer dislocation. When propagating into the epitaxial layer, the two 60° dislocations will separate, and the plan-view observation along $[001]$ will show two parallel $\{100\}$ additional planes, which result in a total Burgers vector of $a[100]$, as schematically shown in Fig. 5(c).

After determining the Burgers vector of the threading dislocations, we can now understand the relations between the pattern of the extra moiré fringes and the threading dislocations. According to the relation of the Burgers vector and moiré fringe: $|g \cdot b| = n$, where g is the diffraction vector, b is the Burgers vector, and n is the number of the extra half moiré fringes,²⁵ we can see that the 60° dislocation with a Burgers vector of $\frac{a}{2}[101]$ exhibits in 2 extra half moiré fringes (lying in $[110]$ and $[1\bar{1}0]$ directions); the Lomer dislocation with a Burgers vector of $\frac{a}{2}[110]$ shows 2 extra half moiré fringes (in the $[110]$ direction); and 60° dislocation pair with Burgers vector of $\frac{a}{2}[101]$ and $\frac{a}{2}[10\bar{1}]$ results in 4 extra half moiré fringes (2 of them lying along $[110]$ and the others in $[1\bar{1}0]$).

In summary, the above observations show that three kinds of defects (or imperfections) of the misfit dislocation network result in three types of threading dislocation: the half period shift of Lomer dislocation, which are related to the 60° dislocation lead to a mixed type threading dislocation; the extra Lomer misfit dislocation generates an edge type threading dislocation, which rapidly dissociates into two mixed type threading dislocations. The third type of

imperfection, which is related to a 60° dislocations pair, leads to the formation of pair of mixed type threading dislocations, which also separate during the growth. Finally, only isolated mixed type threading dislocation are observed to reach the surface of a 600 nm GaSb epitaxial layer. Therefore, it can be pointed out that the main sources of threading dislocations are these misfit dislocation network imperfections, which have been identified. And, the dominant propagation mechanism is the conventional glide inside $\{111\}$ lattice planes subsequent to the decomposition of all initial Lomer and pairs of 60° dislocations into pure mixed type threading dislocations.

This work was supported by the national research agency under project MOS35, Contract No.: ANR-08-NANO-022. One of the authors, S. Kret, acknowledges the European Regional Development Fund within the Innovative Economy Operational Program 2007-2013, Grant No. POIG.02.01-00-14-032/08.

¹B. R. Bennett, R. Magno, J. B. Boos, W. Kruppa, and M. G. Ancona, *Solid-State Electron.* **49**, 1875 (2005).

²S. Sharan and J. Narayan, *J. Appl. Phys.* **66**, 2376 (1989).

³A. Vilà, A. Cornet, J. R. Morante, M. Loubradou, R. Bonnet, Y. González, L. González, and P. Ruterana, *Philos. Mag. A* **71**, 85 (1995).

⁴R. E. Mallard, P. R. Wilshaw, N. J. Mason, P. J. Walker, and G. R. Booker (presented at Microsc. Semiconduct. Mater. 1989) Inst. Phys. Conf. Ser. **100**, 331 (1989).

⁵A. Vilà, A. Cornet, J. R. Morante, P. Ruterana, M. Loubradou, and R. Bonnet, *J. Appl. Phys.* **79**, 676 (1996).

⁶P. J. Taylor, W. A. Jesser, J. D. Benson, M. Martinka, J. H. Dinan, J. Bradshaw, M. Lara-Taysing, R. P. Leavitt, G. Simonis, W. Chang, W. W. Clark, and K. A. Bertness, *J. Appl. Phys.* **89**, 4365 (2001).

⁷A. M. Rocher, *Solid State Phenom.* **19–20**, 563 (1991).

⁸S. Huang, G. Balakrishnan, and D. L. Huffaker, *J. Appl. Phys.* **105**, 103104 (2009).

⁹W. Qian, M. Skowronski, R. Kaspi, M. De Graef, and V. P. Dravid, *J. Appl. Phys.* **81**, 7268 (1997).

¹⁰Y. Wang, P. Ruterana, S. Kret, J. Chen, S. El Kazzi, L. Desplanque, and X. Wallart, *Appl. Phys. Lett.* **100**, 262110 (2012).

¹¹W. Qian, M. Skowronski, and R. Kaspi, *J. Electrochem. Soc.* **144**, 1430 (1997).

¹²J. M. Kang, M. Nouaoura, L. Lassabatère, and A. Rocher, *J. Cryst. Growth* **143**, 115 (1994).

¹³J. Narayan and S. Oktyabrsky, *J. Appl. Phys.* **92**, 7122 (2002).

- ¹⁴J. G. Zhu and C. B. Carter, *Philos. Mag. A* **62**, 319 (1990).
- ¹⁵A. Rocher, M.-N. Charasse, B. Bartenlian, and J. Chazelas, *J. Phys. Colloq.* **51**(C1) 915 (1990).
- ¹⁶P. Komninou, J. Stoemenos, G. P. Dimitrakopoulos, and T. Karakostas, *J. Appl. Phys.* **75**, 143 (1994).
- ¹⁷S. F. Fang, K. Adomi, S. Iyer, H. Morkoç, H. Zabel, C. Choi, and N. Otsuka, *J. Appl. Phys.* **68**, R31(1990).
- ¹⁸S. J. Pennycook, in *Advances in Imaging and Electron Physics* (Elsevier, 2002), pp. 173–206.
- ¹⁹E. Carlino and V. Grillo, *Phys. Rev. B* **71**, 235303 (2005).
- ²⁰C. T. Koch, *Determination of Core Structure Periodicity and Point Defect Density Along Dislocations*, (Arizona State University, 2002).
- ²¹M. J. Hÿtch, E. Snoeck, and R. Kilaas, *Ultramicroscopy* **74**, 131 (1998).
- ²²S. Kret, P. Ruterana, A. Rosenauer, and D. Gerthsen, *Phys. Status Solidi B* **227**, 247 (2001).
- ²³S. Kret, PawełDłużewski, P. Dłużewski, and E. Sobczak, *J. Phys.: Condens. Matter* **12**, 10313 (2000).
- ²⁴D. Hull and D. J. Bacon, *Introduction to Dislocations* (Elsevier, 2011).
- ²⁵G. A. Bassett, J. W. Menter, and D. W. Pashley, *Proc. R. Soc. London Ser. A* **246**, 345 (1958).